Solid-state amorphization in Ni/Nb mutilayers studied by molecular-dynamics simulation together with experiments

2000 J. Phys.: Condens. Matter 12 6991

(http://iopscience.iop.org/0953-8984/12/31/301)

J. Phys.: Condens. Matter **12** (2000) 6991–7004. Printed in the UK PII: S0953-8984(00)12582-2

Solid-state amorphization in Ni/Nb mutilayers studied by molecular-dynamics simulation together with experiments

Q Zhang, W S Lai, G W Yang and B X Liu†

Department of Materials Science and Engineering, Tsinghua University, Beijing 100084, People's Republic of China
and
National Laboratory of Solid-State Microstructure, Nanjing University, Nanjing 210093, People's Republic of China

E-mail: dmslbx@tsinghua.edu.cn

Received 14 March 2000, in final form 5 June 2000

Abstract. Based on an embedded-atom method, an n-body potential is developed for the Ni–Nb system and the potential is then applied in molecular-dynamics simulation to study the detailed process of interfacial reaction in an Ni–Nb sandwich model. It turns out that the solid-state amorphization is initiated by interface-crossing atomic migration and governed by diffusion-limited reaction in the Ni–Nb system characterized by a negative heat of formation. The simulation results are confirmed by thermal annealing experiments conducted at medium temperatures.

1. Introduction

Solid-state amorphization (SSA) in mutilayers consisting of two pure crystalline metals was first observed by Schwarz and Johnson in the Au–La system in 1983 [1]. The emergence of SSA is a breakthrough physical concept in the field of amorphous solids, since it was proved that at medium temperatures, simple thermally excited interdiffusion of two elemental metals can result in the formation of an amorphous phase. Consequently, the crystal-to-amorphous transition upon solid-state reaction is different in kinetics from that involved in ion mixing, which is a sort of quenching-like process far from equilibrium, though solid-state reaction and ion mixing both start with multiple metal layers. In the last 15 years, some other binary metal systems have been studied by experiments concerning the phase transition upon solid-state reaction and the glass-forming ability in thin films [2, 3]. Meanwhile, a clear understanding of solid-state interfacial reaction at an atomic scale is still lacking. In recent years, molecular-dynamics (MD) simulation has been performed to study SSA and proved to be a powerful means in modelling the atomistic mechanism involved in solid-state interfacial reaction [4, 5].

It is found that for SSA, the annealing temperature should be high enough to allow a sufficiently fast interdiffusion of the metal atoms to cross the interfaces, yet still low enough to avoid the nucleation of any possible crystalline phase during the reaction time. For example, the reaction temperature of the above mentioned Au–La system was as low as 80 °C [1], as the system has a large negative heat of formation ($\Delta H_f = -108$ kJ mol^{-1}) which could drive

† Addressee for correspondence.

0953-8984/00/316991+14$30.00

the atoms to diffuse into their partner lattices [6]. For another system, i.e. the Ni–Ti system with a heat of formation of $\Delta H_f = -52$ kJ mol^{-1} [6], the reaction temperature was observed to be about 350 °C [2]. It should be noted that in the semi-quantitative Miedema model, the heat of formation is calculated as a sum of the chemical, structural and elastic terms. With the model, the Gibb's free energy of the solid-solution, amorphous, intermetallic compounds can be calculated; the value of the heat/enthalpy of formation therefore represents the ability of alloying between the two constituent metals. It is known that the Ni–Nb system, having a negative heat of formation ($\Delta H_f = -45$ kJ mol^{-1}) [6], is a typical glass-forming system consisting of an early and a late transition metal and that amorphization has been achieved through either liquid melting quenching [7] or ion beam mixing [8, 9]. However, there is no neat result of solid-state amorphization reported for the Ni–Nb system, even though the solid-state reaction has been studied by thermal annealing of the Ni–Nb multilayered films at a temperature of 400 °C [7]. The present study is devoted to investigating the detailed process of solid-state amorphization in the Ni–Nb system as a representative one, by performing both MD simulation and experiment. Firstly, an n-body Ni–Nb potential is developed under an embedded-atom method (EAM) [10], since there is no such potential available in the literature. MD simulation is then performed based on the potential to reveal the details of solid-state interfacial reaction of the Ni–Nb multilayers upon isothermal annealing at medium temperatures. A steady-state thermal annealing experiment is also conducted and the observations are compared with the simulation results. We present, in this paper, the construction of the EAM potential, the simulation model and characterization methods, the major results of simulation and experiment together with some discussion.

2. Construction of an n-body potential

To overcome the limitations of the pair potentials, the n-body models have been developed and used successfully in quite broad fields of computer simulation. In 1983, Daw and Baskes first proposed an approach named the embedded-atom method (EAM), which is based on density functional theory, and the method has been used extensively for metals [10, 11]. Subsequently, similar models in different formats were presented by other researchers, such as the second-moment approximation of the tight-binding scheme (TB-SMA) and the formalism proposed by Finnis and Sinclair [12, 13]. Among these approaches, the EAM potential is probably close to a realistic one, since the total energy of a system is designed to follow the equation of state formulated by Rose *et al* [14] in the fitting procedure and thus the physical properties away from equilibrium state are already fitted in the EAM. Accordingly, the potential for pure metals can directly be applied to metallic alloys, while the potentials constructed under most of other formalisms cannot. In the original form of Daw and Baskes, the potential was in a non-analytical form, which was inconvenient for calculation. For computation efficiency, we adopt, in the present work, the analytic form proposed by Johnson and Oh for bcc metals and the form developed recently by Cai and Ye for fcc metals [15, 16] as Nb is of bcc and Ni is of fcc structure.

In the framework of the EAM approach, the total energy of the system of N atoms is described as

$$E_{tot} = \sum_i F_i(\rho_i) + \sum_{i>j} \phi(r_{ij}) \tag{1}$$

$$\rho_i = \sum_{j(\neq i)} f(r_{ji}) \tag{2}$$

where E_{tot} is the total energy, $F_i(\rho_i)$ is the embedding energy, ρ_i is the total electron density at atom i due to all other atoms, $\varphi(r_{ij})$ is the pair potential between atoms i and j and $f(r_{ij})$ is the atom electron density for atom i contributed by atom j. In Johnson's and Cai's models, the embedding functions $F(\rho)$ are actually quite similar except an additional linear term proposed by Cai, and it can be expressed by

$$F(\rho) = -F_0\left[1 - \ln\left(\frac{\rho}{\rho_e}\right)^n\right]\left(\frac{\rho}{\rho_e}\right)^n + F_1\left(\frac{\rho}{\rho_e}\right). \tag{3}$$

For the bcc model F_1 equals 0, while for the fcc model F_1 is an adjustable parameter. In two models, $F_0 = E_c - E_v^f$, where E_c and E_v^f are the cohesive energy and vacancy formation energy, respectively. ρ_e represents the host electron density at an equilibrium state. It is thus convenient to combine the two models together for the Ni(fcc)–Nb(bcc) system. Since the embedding function $F(\rho)$ is universal and does not depend on the source of the host electron density, the electron density functions $f_{Ni}(r)$ and $f_{Nb}(r)$, the embedding energy functions $F_{Ni}(\rho)$ and $F_{Nb}(\rho)$ are assumed to be transferable from two monatomic systems to one binary metal system, as for the pair potential functions $\varphi_{Ni-Ni}(r)$ and $\varphi_{Nb-Nb}(r)$. The electron-density scaling factor f_e, which is taken as unity for a pure metal system but cannot be cancelled in the binary metal system, is determined by the equation $f_e = E_c/\Omega$ (E_c is the cohesive energy and Ω is the atom volume) as pointed out by Johnson [17]. In Cai's original scheme, the cutoff distance is taken as $r_{cut} = 1.65\,a_0$ (a_0 is the equilibrium lattice constant), which is between the fifth and sixth neighbours. In our case, the r_{cut} of Ni is assumed to be between the second- and third-neighbour distances, which is similar to that adopted by Johnson for bcc metals. The parameters in the Ni potential should therefore be refitted by an optimization procedure. In Cai's model, the atomic electron density $f_{Ni}(r)$ and pair potential $\varphi_{Ni-Ni}(r)$ are defined as

$$f(r) = f_e \exp[-\chi(r - r_e)] \tag{4}$$

and

$$\varphi(r) = -\alpha[1 + \beta(r/r_a - 1)]\exp[-\beta(r/r_a - 1)]. \tag{5}$$

From the above equations, there are in total five potential parameters (χ, α, β, F_1 and r_a) for Ni–Ni interaction. The fitting results obtained in this study are displayed in table 1. Although our present model includes no long range force like that in the original format, the major intrinsic properties can still be reproduced and the deduced equation of state is in good agreement with Rose's. The potential parameters for Nb–Nb interaction are adopted from Johnson's data, which are not listed here. The remaining function that needs to be developed is the cross pair potential function $\varphi_{Ni-Nb}(r)$, which is assumed as

$$\begin{aligned} \varphi(r) &= (r - c)^2(c_0 + c_1 r + c_2 r^2 + c_3 r^3 + c_4 r^4) && r \leqslant c \\ &= 0 && r > c. \end{aligned} \tag{6}$$

Table 1. The potential parameters for Ni–Ni and Ni–Nb.

Ni–Ni		Ni–Nb	
F_0 (eV)	2.97	c	3.8
χ (Å^{-1})	2.821 497	c_0	51.683 55
α (eV)	0.6080	c_1	−69.7978
β	6.46	c_2	34.2912
F_1 (eV)	1.58	c_3	−7.189 241
r_a (Å)	2.1965	c_4	0.523 113
r_{cut} (Å)	3.9		

The format is similar to that proposed by Finnis and Sinclair (FS) and takes a polynomial form extending up to r^6, instead of a quartic form in the original FS formalism, for computational flexibility in obtaining a relevant potential [13]. Because of the shortage of the experimental data for the equilibrium Ni–Nb alloy phases, the parameters in $\varphi_{Ni-Nb}(r)$ are derived by using some physical properties obtained with linear muffin-tin orbital (LMTO) calculation for four Ni–Nb metastable crystalline phases, among which three have been observed in experiments [8, 9, 18]. The fitting results are also listed in table 1. Employing the derived Ni–Nb potential, the cohesive energies, the lattice constants and the bulk moduli are reproduced for the above mentioned four metastable crystalline phases and listed in table 2. The values used in fitting the potential are denoted by asterisks and other properties calculated for testing the potential are in good agreement with those from first principles calculation. It is known that the absolute values of cohesive energies of the related alloy phases derived from the atomic potential are not precise; however, their sequence can reflect the relative stability of the alloy phases at same composition. In addition, the lattice constants of the equilibrium β-Ni_3Nb phase, that has not been employed in the fitting procedure, are reproduced by the potential and agree well with the experimental values within an error of 2% [19]. Besides, the melting point, as a dynamics property, of the β-phase is obtained through MD simulation of its crystal model with periodic boundary condition as shown in figure 1. One sees from the figure that there is an abrupt change for both molar enthalpy H and volume V at a temperature around 1750 K. This temperature can therefore be regarded as the melting point, which is well compatible with the experimental value of 1703 K [20]. For a further test of the potential, we remove the translational periodicity constraints and find that the crystalline structure of β-Ni_3Nb phase does not become disordered after running. For all these metastable and equilibrium alloy phases, the Rose equation can also be reproduced by the derived potential. All the above discussion suggests that the n-body potential so constructed is of relevance in describing the atomic interactions for the Ni–Nb system.

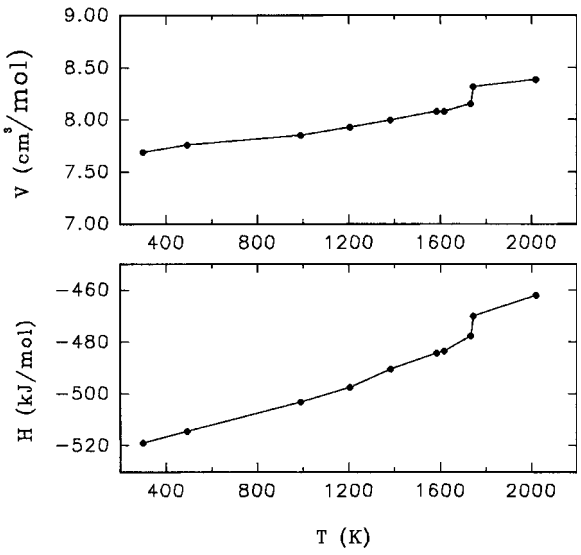

Figure 1. The variations of molar enthalpy and volume of β-Ni_3Nb phase versus temperature.

Table 2. The comparison of physical properties derived from the constructed potential with those from LMTO calculation. Cohesive energy in eV/atom, lattice constant in Å. (From experiments, for Ni_3Nb $D0_{19}$, $c/a = 1.60$; $NiNb_3$ $D0_{19}$, $c/a = 1.63$. The data used in fitting are denoted by asterisks.)

		$-E_c$		B		A		
System	Structure	LMTO [18]	This work	LMTO	This work	LMTO	Expt	This work
Ni_3Nb	$D0_{19}$	5.586*	5.470	2.57*	2.20	2.637*	2.53 [6]	2.577
	$L1_2$	5.439*	5.425	2.54	2.29	3.717*		3.629
$NiNb_3$	$D0_{19}$	6.711	6.737	2.25	1.5	2.915	2.91 [7]	2.891
	$L1_2$	6.724	6.738	2.23	1.5	4.124	4.11 [7]	4.078

3. Computation, model and characterization

Employing the constructed potential, molecular-dynamics (MD) simulation is then conducted to study the detailed process of solid-state interfacial reaction in the Ni–Nb system. The simulation is carried out with the Parrinello–Rahman constant pressure molecular-dynamics scheme [21] and the equations of motion are solved using a fourth-order predictor–corrector algorithm of Gear with a time step $t = 5 \times 10^{-15}$ s. The pressure is fixed at zero.

To represent the multilayered films frequently employed in experiments, we adopt a sandwich model with periodic boundary conditions. The sandwich model is constructed by stacking Ni(001) atomic planes and Nb(001) atomic planes along the z axis and parallel to the x–y plane. The crystalline direction ⟨100⟩ of fcc Ni and ⟨100⟩ of bcc Nb are arranged to be parallel to the x and y axes with the unit distances of 3.52 and 3.30 Å, respectively, leading to a size difference ratio of 1.067. Considering the number of atoms in the simulation model to be within a manageable scale, the numbers of Ni and Nb unit cells in the x–y plane are selected to be $11 \times 11 = 121$ and $12 \times 12 = 144$, respectively, resulting in a lattice difference ratio of $12/11 = 1.091$, which is reasonably close to the above mentioned real situation. Consequently, the periodic conditions along the x and y directions are set by the lattice parameters of Nb and the interface area of the simulation model is of 39.6×39.6 Å^2. Naturally, such setting will cause a misfit for the lattice dimension of Ni and will result in a 2.2% density decrease of Ni in the model. As pointed out by Mura *et al* in their simulation of an Ni–Zr multilayer upon loading [22], such a density reduction would only have a minor influence on the simulation results. After the numbers of atoms in the atomic planes are fixed, the overall atomic composition ratio can be adjusted by varying the numbers of the Ni and Nb atomic planes along the z direction. It has been shown that when the alloy compositions are located at or near the intermetallic compounds frequently featuring complicated crystalline structures, the amorphous phase is readily formed, because the crystallization of such complicated compounds is frustrated in most of the non-equilibrium processes [23]. In the present study, we therefore design the overall composition of the sandwich model to be as close as possible to the intermetallic compound Ni_3Nb, with consideration of manageability. Consequently, the model consists of two bcc Nb(001) planes (Nos 1, 2), eight fcc Ni(001) planes (Nos 3–10) and two bcc Nb(001) planes (Nos 11, 12) along the z direction, leading to an overall composition of 22.93 at.% of Nb. In fact, an Ni–Nb alloy with 22.93 at.% of Nb is in the range of the intermetallic compound Ni_3Nb emerging in the equilibrium phase diagram. For the z direction, a periodic boundary condition is also employed and thus the two Nb lattices in the sandwich model are adhered together to form a united lattice. Incidentally, a sandwich model is easier to handle the interface and the boundary separately than a bilayer model also imposed with a periodic boundary. We use [2Nb/8Ni/2Nb] to signify the sandwich model. Figure 2 gives a projection

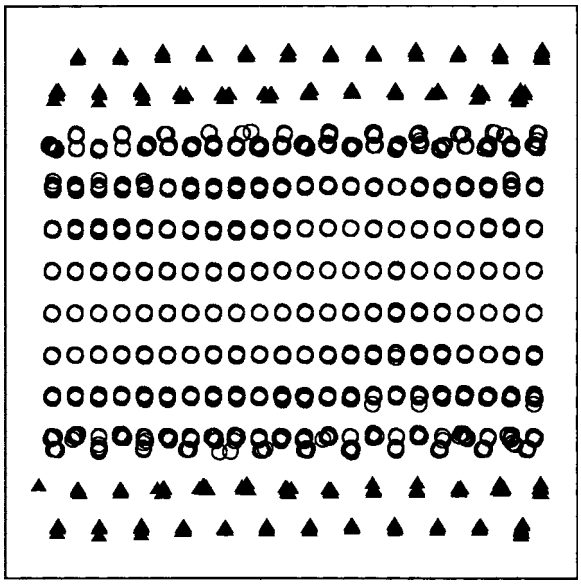

Figure 2. The projection of the atomic positions on the x–z plane of the sandwich-model at 0 K. Open circles: Ni. Filled triangles: Nb.

for the atomic positions on the x–z plane after equilibrating at 0 K. To examine the additional energy of the model relative to the equal amount of Ni and Nb atoms in their infinite single crystals, we calculate the additional energy per atom E^A by

$$E^A = \frac{E^m - N_{Ni}E_{Ni}^{Coh} - N_{Nb}E_{Nb}^{Coh}}{N_{Ni} + N_{Nb}} \tag{7}$$

where E^m is the lattice energy of the sandwich model and in this case equal to $-12\,720$ eV, N_{Ni} and N_{Nb} are the numbers of Ni and Nb atoms in the sandwich model, being 1936 and 576, respectively, and E_{Ni}^{Coh} and E_{Nb}^{Coh} are the cohesive energies of Ni and Nb, being -4.44 and -7.47 eV/atom, respectively. It can thus be calculated that the model has an additional energy of 0.07 eV/atom, which should be attributed to the interfacial energy originates from the chemical and elastic interaction between Ni and Nb atoms/lattices.

Another two sandwich models, denoted by [4Nb/8Ni/2Nb] and [6Nb/10Ni/4Nb], are constructed to reveal the effect of model size on the interfacial reaction. Besides, we also construct a bilayer model [8Ni/8Nb] with a free boundary condition on the z direction, in which there is only one interface and no interaction of interfaces exists.

To describe the detailed process of interfacial reaction, the most direct and convenient way is to display graphically the atomic positions at various times onto a projected plane, e.g. the x–z plane. An alternative way is to display the density profiles of each metal species, i.e. the normalized atom distributions, along the z direction $\rho_\alpha(z)$, which can provide the local structural and compositional information of the model.

To monitor the phase evolution in the model, two quantitative methods are employed. The first one is so called pair-correlation function analysis, which is commonly recognized to give convincing evidence for distinguishing the structure to be either crystalline or amorphous. To calculate the pair-correlation function $g(r)$, each atom in turn is imagined to be at the centre of a series of concentric spheres. The atomic density is defined to be the number of atoms in each spherical shell divided by the volume of that shell, taking consideration of those periodic image

atoms located outside the block. In the present study, the results are obtained by averaging over all the atoms within 200 time steps. The $g(r)$ is obtained by the following formula:

$$g(r) = \frac{\rho(r)}{\rho_0} \tag{8}$$

where $\rho(r)$ denotes the atomic density at $r = |\boldsymbol{r}|$, $r = 0$ defines the position of a reference atom and ρ_0 is an average atomic density in the whole model. The second method is the planar structure factors, which represent the degrees of disorder in the atomic planes, i.e. the original crystal planes. The planar structure factor $S(\boldsymbol{k})$ is evaluated at each time step to detect the changing of ordering in each atomic plane with increasing simulation time. The $S(\boldsymbol{k})$ is the Fourier transformation of the density in each crystallographic plane parallel to the x–y plane and is defined by Phillpot *et al* as [24]

$$S(\boldsymbol{k}, z) = \left\langle \frac{1}{N_Z^2} \left| \sum_{j=1}^{N_Z} \exp(\mathrm{i}\boldsymbol{k} \cdot \boldsymbol{r}_j) \right|^2 \right\rangle \tag{9}$$

where z labels the crystal plane to which the point $\boldsymbol{r}_j$ belongs at initial configuration, and $\boldsymbol{k}$ is an arbitrary vector of the planar reciprocal lattice (in our case, $\boldsymbol{k} = (1, 1)$ is used). Accordingly, the planar structure factor $S = 1$ refers to an entirely ordered crystal while $S = 0$ is for a completely disordered state.

4. Results and discussion

A pre-running of the sandwich-model [2Nb/8Ni/2Nb] is conducted at room temperature (27 °C) for 5000 MD time steps, corresponding to 25 ps, to reach an equilibrium state as an initial atomic configuration. The initial state is similar to that shown in figure 2 except that the atoms, especially those near the interfaces, have a little thermal vibration. The lattice energy of the initial state is −12 714 eV, which is a little bit higher than that at 0 K because of elevating the temperature. The model is then heated up at a rate of 4×10^{13} °C s^{-1} to various temperatures ranging from 300 to 500 °C, at which isothermal annealing is simulated to investigate the interfacial reaction. As the velocities of the atoms will change during annealing, a time-to-time re-scaling of the velocities to the assigned temperature is executed at every 10 time steps, if an average deviation from the assigned temperature is over 1 °C. It is known that the Gear method may lead to some energy drift in the simulation. In our study, if no periodic rescaling of temperature is done during running at 27 °C for 25 ps, the total energy of the sandwich model remains constant within a 1% error which have no significant influence.

We now discuss the simulation results obtained by 500 °C isothermal annealing of the sandwich model as a typical example. It should be noted that the value of 4×10^{13} °C s^{-1} is the heating rate to increase temperature artificially within each time step. Since the atoms in the model would somehow relax and modulate, the actual heating rate is less than 4×10^{13} °C s^{-1}. In simulation, the temperature of model is compared to the designed one every time step and when they are equal, the heating procedure will stop. In fact, it takes 4801 MD time steps for the model to reach the designed 500 °C. Figure 3 shows the changing of the normalized density profiles, $\rho_\alpha(z)$, of each metal species along the z direction, perpendicular to the interface, upon isothermal annealing at 500 °C with increasing time steps. It can be seen that after 4801 MD steps, about 24 ps, when the model is just heated up to 500 °C, some Ni (Nb) atoms near the interfaces diffuse into the Nb (Ni) lattice. After 50 ps, more atoms have diffused into the partner lattices and disordering is thus induced in the respective atomic planes. With increasing simulation time, the density profiles $\rho_\alpha(z)$ for Ni and Nb become more uniform, as evidenced by the curves calculated at 500 ps. One sees clearly that mutual diffusion, which

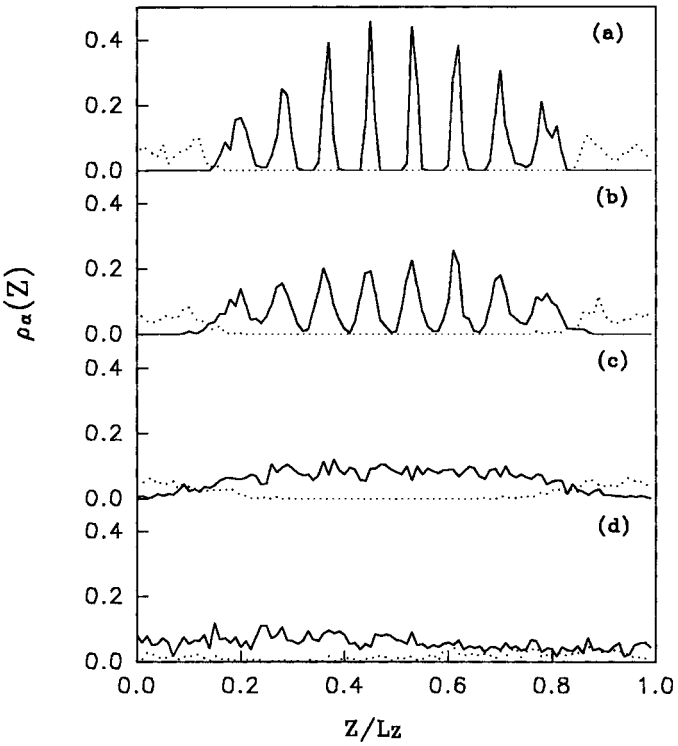

Figure 3. The calculated density profiles, $\rho_\alpha(z)$, of each species along the z direction, for (a) the initial state; (b) just heating up to 500 °C; (c) annealing at 500 °C after 50 ps; (d) annealing after 500 ps. $\rho_{Ni}(z)$ is represented by a solid line and $\rho_{Nb}(n)$ by a dotted line. The ordinate is in arbitrary units. The periodic boundary condition is imposed in the z direction.

is defined as the interface-crossing migration of Ni and Nb atoms, does take place at 500 °C. The structural change in the Ni–Nb sandwich model is also verified by the calculation of the planar structure factors $S(\boldsymbol{k})$ for each atomic plane, as shown in figure 4. In the initial state, $S(\boldsymbol{k})$ are about 0.8 except four atomic planes at the interfaces. After heating up the $S(\boldsymbol{k})$ values of all crystalline planes decrease a little, and after annealing for 100 ps, they all become less than 0.1, suggesting that the sandwich model is completely disordered. After annealing for an additional 400 ps, i.e. the total annealing time is 500 ps, a unique disordered phase is obtained in the sandwich model. Figure 5 gives a snapshot of the projection of the atomic positions at this moment on the x–z plane, which illustrates a completely disordered state. To give sound evidence confirming a resultant disordered structure, the total and partial pair correlation functions for the initial state and the states after annealing at 500 °C for 50 and 500 ps are calculated and displayed in figure 6. Obviously, the strength of the first Nb–Ni $g(r)$ peak increases distinctly, suggesting that a considerable amount of alloying has taken place in the Ni–Nb sandwich model, while those crystalline peaks for the total, Ni–Ni and Nb–Nb $g(r)$ at long distance disappear gradually and the curves eventually feature a shape commonly known for an amorphous state. Furthermore, to illustrate the changing of the atomic surroundings of the Ni and Nb atoms before and after annealing, the coordination numbers are calculated by taking the integral of $4\pi\rho_0 r^2 g(r)$ up to the first minimum, where ρ_0 is the number density of the model. The calculated results are displayed in figure 7. One sees that during annealing, the coordination numbers for Ni–Ni and Nb–Nb decrease from 10.77 to

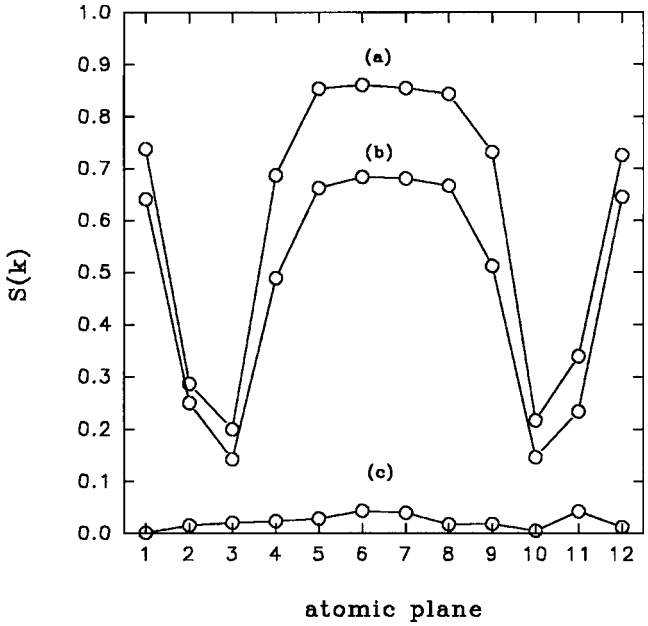

Figure 4. The planar structure factors $S(k)$: (a) the initial state; (b) just heating up to 500 °C; (c) after annealing for 100 ps.

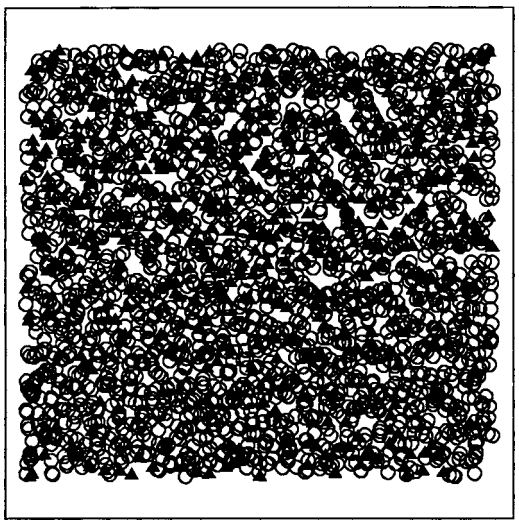

Figure 5. A snapshot of projection of the atomic positions on the x–z plane after annealing the sandwich model at 500 °C for 500 ps. Open circles: Ni. Filled triangles: Nb.

4.73 and from 11.08 to 3.66, respectively, while those numbers for Ni–Nb and Nb–Ni increase from 1.07 to 3.58 and from 3.59 to 12.30, respectively, indicating that significant diffusion and alloying have taken place. One may question why the coordination numbers of the Ni–Ni and Nb–Nb of the initial stage are not exactly 12 and eight, respectively. In fact, for the Nb–Nb bcc structure, the positions of the first- and second-nearest neighbours are very close, which

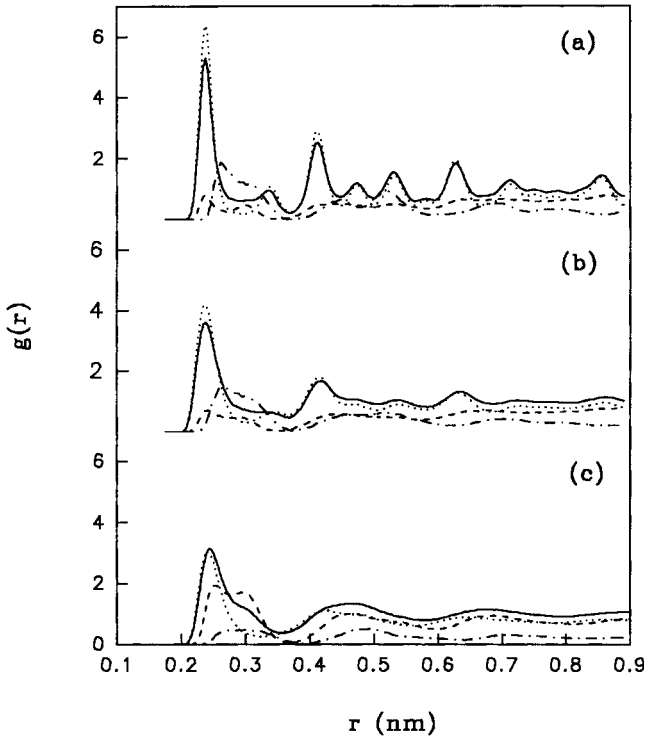

Figure 6. Partial and total pair correlation functions for the initial state (a) and the state after 500 °C annealing for (b) 50 ps and (c) 500 ps. The solid line is for total $g(r)$; the short dashed line is for Nb–Ni $g(r)$; the dotted line is for Ni–Ni $g(r)$ and the dot–dashed line is for Nb–Nb $g(r)$.

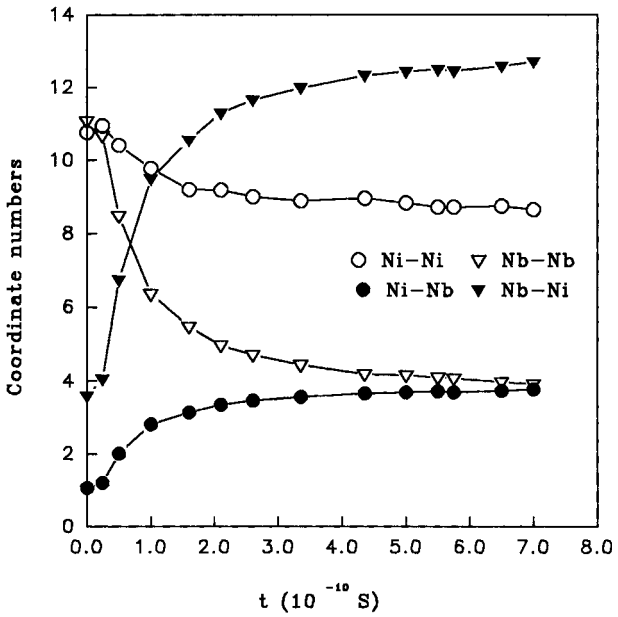

Figure 7. Variation of the coordination numbers versus time step during isothermal annealing of the Ni–Nb multilayers at 500 °C. The coordination numbers are obtained by taking an integral of $4\pi\rho_0 r^2 g(r)$ up to the first minimum, where ρ_0 is the number density of the model system.

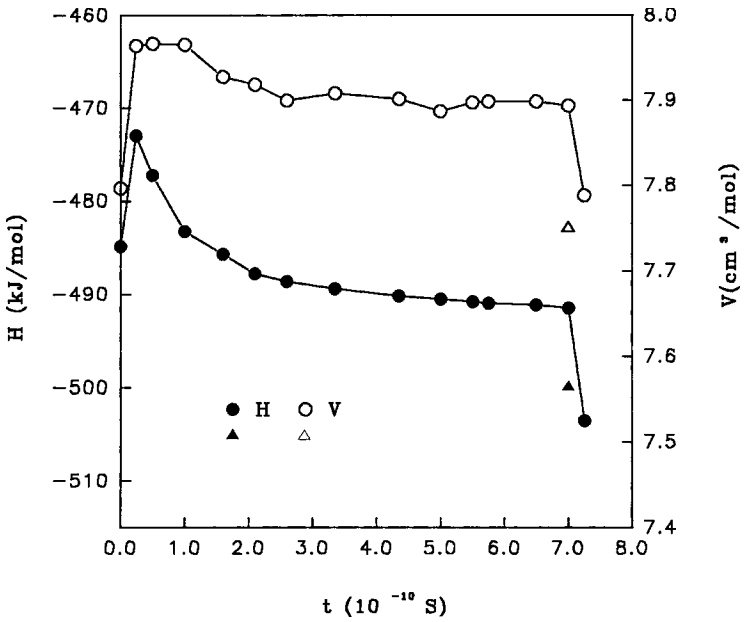

Figure 8. The variations of the enthalpy and the volume of the system versus time step during isothermal annealing of the Ni–Nb multilayers at 500 °C. The increases of the values at initial stage correspond to the elevating of temperature from 27 to 500 °C and the decreases at the terminal stage correspond to the quenching process from 500 to 27 °C. The values of the equilibrium crystalline phase are denoted by triangles.

results in a coordination number of 14. Considering in total four atomic planes consisting of Ni and Nb at the Ni–Nb interfaces, both the Ni and Nb coordination numbers decrease to the above mentioned values.

The variation of the enthalpy and the volume of the sandwich model upon annealing are calculated and shown in figure 8. The increases of the enthalpy and volume before a simulation time of 24 ps are due to the heating of the model from 27 °C up to 500 °C. It can be seen that the enthalpy is declining and the volume is relaxing to a stable state during isothermal annealing, indicating the process of diffusion, alloying and amorphization is accompanied by a decrease of enthalpy. It is noted as well from the figure that the enthalpy and volume both change significantly during a period of 50–100 ps. These changes are in accordance with a considerable variation of the coordination numbers (figure 7), suggesting that mutual diffusion and alloying take place mainly during this time period. Furthermore, the resultant amorphous phase is quenched to 27 °C at a rate of 4×10^{13} °C s^{-1}, and the molar enthalpy and volume of the amorphous phase at room temperature are also shown in figure 8. From a thermodynamic point of view, for the binary metal systems with a negative ΔH_f, such as the Ni–Nb system, the negative ΔH_f is responsible for driving the atoms to mix and alloy each other. Explicitly speaking, the free energy of the amorphous state should be more negative for that of the initial multilayered films consisting of two crystalline metals in the respective layers. The simulation results show that the molar enthalpy of the amorphous alloy is about 19 kJ mol^{-1} (corresponding to 0.20 eV/atom) lower than that of the sandwich model and this value may be regarded as the formation enthalpy of the amorphous phase at this composition (22.93 at.% of Nb). Besides, the molar volume of the amorphous phase is about 1% greater than that of the sandwich model, which is attributed to an excess free volume predicted by theory for the

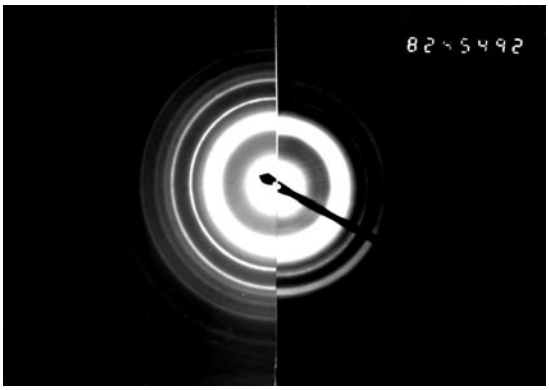

(a) (b)

Figure 9. The selected-area diffraction patterns for Ni/Nb mutilayers: (a) the initial state and (b) after consecutive annealing from 250 to 400 °C (a temperature raising step is 50 °C, staying time is 60 minutes at every step).

amorphous phase versus its crystal counterpart [23]. The molar enthalpy and volume are also computed for the equilibrium Ni–Nb phase at an alloy composition of 22.93 at.% of Nb with a $D0_a$ structure at 500 °C for comparison and the results are also shown in figure 8. Obviously, the equilibrium phase has more negative enthalpy than the amorphous state, yet its nucleation and growth are kinetically hindered, because of its complicated structure, the low reaction temperature as well as the short time period for reaction. As the amorphous phase is in a metastable state, it can be expected that after annealing for very long time, it should transform into the corresponding equilibrium phase. However, it is very difficult for MD simulation to represent such re-crystallization process. In short, the simulation results indicate that in the solid-state interfacial reaction, the atoms migrate crossing the interfaces and try to adopt a lower energy of an equilibrium crystalline phase via alloying, yet such structural evolution is kinetically frustrated, leading to the formation of an amorphous phase as an intermediate state.

MD simulations are also conducted at 400 and 300 °C for respective time steps. In the case of annealing at 400 °C, diffusion driven amorphization proceeds similarly, yet with a slower speed than that in the case of 500 °C. While decreasing the annealing temperature to 300 °C, little mutual diffusion can be observed and amorphization is reluctant to proceed after running up to 200 ps. The onset temperature of amorphization in the Ni–Nb system is therefore deduced to be lower than 400 °C.

In the above model [2Nb/8Ni/2Nb] model, there are in total four 4 Nb atomic planes. To increase the atomic planes of Nb, we construct another sandwich model [4Nb/8Ni/2Nb], in which two interfaces are set between the atomic planes Nos 4, 5 and Nos 12, 13, respectively. After isothermal annealing at 500 °C for 400 ps, only a little mutual diffusion can be visualized and the multilayers retain crystalline structure. With equation (7), the additional energy of the model is calculated to be 0.056 eV/atom, which is less than that of model [2Nb/8Ni/2Nb], indicating that the free energy of the model somehow depend on the system size and have influenced the interfacial reaction.

In the experiment, it has been observed that in some multilayers, SSA could take place upon annealing when the interfacial layers were in a disordered state and that the interfacial reaction was completely suppressed if coherent interfaces emerged [2], implying that a sharp interface may act as a nucleation barrier against interfacial reaction. In the model [4Nb/8Ni/2Nb], we also form a disordered interfacial structure of the multilayers like that observed in experiments

by randomly exchanging 90 Ni and 90 Nb atoms in two interfaces. The model is equilibrated at 27 °C for 25 ps to an initial state, which is then heated up to 500 °C for annealing. In the initial state, the Ni and Nb atomic planes retain in good crystalline states and almost no alloying atoms have diffused into its partner lattice except the four interfacial atomic planes in which chemical disorder is already preset. After isothermal annealing at 500 °C for 1.25 ns, a uniform amorphous structure is obtained. Apparently, the interfacial reaction and amorphization does take place in the model with a preset disordered interface.

We now discuss the simulation results of a bilayer-model of [8Ni/8Nb] upon annealing. The unique interface separating the Ni and Nb lattices lies between the atomic planes No 8 and No 9. When a disordered interlayer is preset in Nos 8, 9, after annealing at 500 °C for 1.0 ns, the amorphous layer extends and includes Nos 6–10 atomic planes, indicating that the interation of the interfaces is not necessary for amorphization.

To give experimental evidence of solid-state amorphization in the Ni–Nb multilayered films upon medium temperature annealing, we perform thermal annealing of the Ni/Nb multilayers with various overall compositions in a hot stage attached to a transmission electron microscope and solid-state amorphization is indeed observed under appropriate conditions. Figure 9 shows the selected area diffraction patterns taken for a representative multilayered sample before and after annealing. The annealing is a consecutive procedure beginning at 250 °C and raising 50 °C every 60 minutes and eventually staying at 400 °C for 1 h. Figure 9(a) shows clearly the sharp diffraction lines from a mixture of crystalline Ni and Nb metals in the initial state, while figure 9(b) shows three diffused halos; especially the first halo is quite strong and is situated in the middle of the two strongest diffraction lines of Ni(111) and Nb(110), giving firm evidence that the resultant product is an Ni–Nb amorphous alloy phase.

5. Concluding remarks

In summary, an approximate n-body Ni–Nb potential is constructed and it is able to reproduce some intrinsic physical properties of the Ni–Nb system. Based on the potential, our simulation of the Ni–Nb multilayers reveals that alloying between Ni and Nb layers is driven by mutual atomic diffusion upon isothermal annealing and it in turn results in transforming the original crystalline metals into an amorphous alloy. The simulated solid-state amorphization is confirmed by our isothermal annealing experiments with the respective Ni–Nb multilayered films at relevant temperatures. The compatibility between MD simulation with experimental results concerning solid-state amorphization also lends support to the relevance of the developed potential in describing the atomic interactions in the Ni–Nb system.

Acknowledgment

This project was supported by the National Natural Science Foundation of China.

References

[1] Schwarz R B and Johnson W L 1983 *Phys. Rev. Lett.* **51** 415
[2] Clemens B M 1986 *Phys. Rev.* B **33** 7615
[3] Cotts E J, Meng W J and Johnson W L 1986 *Phys. Rev. Lett.* **57** 2295
[4] Weissmann M, Ramíez R and Kiwi M 1992 *Phys. Rev.* B **46** 2577
[5] Lai W S and Liu B X 1998 *Phys. Rev.* B **53** 6063
[6] de Boer F R, Boom R, Matters W C M, Miedema A R and Niessen A K 1988 *Cohesion in Metals: Transition Metal Alloys* (Amsterdam: North-Holland)
[7] Ruhl R C, Giessen B C, Cohen M and Grant N J 1967 *Acta Metall.* **15** 1693

[8] Zhang Z J, Bai H Y, Qiu Q L, Yang T, Tao K and Liu B X 1993 *J. Appl. Phys.* **73** 1702
[9] Zhang Z J and Liu B X 1994 *J. Appl. Phys.* **75** 4948
[10] Daw M S and Baskes I 1983 *Phys. Rev. Lett.* **50** 1285
[11] Johnson R A 1989 *Phys. Rev.* B **37** 3924
[12] Rosato V, Guillope M and Legrand B 1989 *Phil. Mag.* A **59** 321
[13] Finnis M W and Sinclair J E 1984 *Phil. Mag.* A **50** 45
[14] Rose J H, Smith J R, Guinea F and Ferrante J 1984 *Phys. Rev.* B **29** 2963
[15] Johnson R A and Oh D J 1989 *J. Mater. Res.* **4** 1195
[16] Cai J and Ye Y Y 1997 *Phys. Rev.* B **54** 8398
[17] Johnson R A 1990 *Phys. Rev.* B **41** 9717
[18] Huang X Y, Pan J S and Fan Y D 1997 *Solid State Commun.* **104** 101
[19] Joint Committee on Powder Diffraction Standards (JCPDS) Card No 15-0101
[20] Brandes E A and Brook G B 1992 *Smithells Metals Reference Book* 7th edn (Oxford: Butterworth-Heinemann)
[21] Parrinello M and Rahman A 1981 *J. Appl. Phys.* **52** 7182
[22] Mura P, Demontis P, Suffritti G B, Rosato V and Vittori Antisari M 1994 *Phys. Rev.* B **50** 2850
[23] van den Beukel A and Radelaar S 1983 *Acta Metall.* **31** 419